Title

Molecular Beam Studies of the Photolysis of Allene and the Secondary Dissociation of the C{sub 3}H{sub x} Fragments

Journal

Journal of Chemical Physics, 95(10)

Authors

Anex, W.M.
Jackson, D.S.
Continetti, R.E.
et al.

Publication Date

1991-06-01

LBL-31171
Preprint

Lawrence Berkeley Laboratory
UNIVERSITY OF CALIFORNIA

Materials & Chemical Sciences Division

Submitted to Journal of Chemical Physics

Molecular Beam Studies of the Photolysis of Allene and the Secondary Dissociation of the C_3H_x Fragments

W.M. Jackson

June 1991

Prepared for the U.S. Department of Energy under Contract Number DE-AC03-76SF00098

DISCLAIMER

LBL-31171

Molecular Beam Studies of the Photolysis of Allene and the Secondary Dissociation of the C_3H_x Fragments

W.M. Jackson

Department of Chemistry
University of California
Davis, CA 95616

Deon S. Anex, R.E. Continetti, B.A. Balko, and Y.T. Lee

Department of Chemistry
University of California
Berkeley, CA 94720

and

Chemical Sciences Division
Lawrence Berkeley Laboratory
University of California
Berkeley, CA 94720

June 1991

This work was supported in part by the Miller Foundation, by the Guggenheim Foundation, by the National Science Foundation under Grant No. CHE-9008095, by the DOE Combustion Program, Office of Basic Energy Sciences, under Grant No. DE-FG05-84er-13213, and by the Director, Office of Energy Research, Office of Basic Energy Sciences, Chemical Sciences Division, of the U.S. Department of Energy under Contract No. DE-AC03-76SF00098.

Molecular Beam Studies of the Photolysis of Allene and the Secondary Photodissociation of the C_3H_x Fragments.

W. M. Jackson*,

Department of Chemistry

University of California

Davis, California 95616

Deon S. Anex, R. E. Continetti, B. A. Balko and Y. T. Lee

Department of Chemistry

University of California

Berkeley, California 94720

Abstract

Angle resolved Time of Flight (TOF) measurements of the fragments produced when allene is photolyzed at 193 nm are described. The two primary processes that have been identified from these measurements are the H + C_3H_3 and the H_2 + C_3H_2 channels. The quantum yields for these first steps are 0.89 and 0.11 respectively. Subsequent photolysis of the C_3H_3 radical produces H_2 + C_3H, C_3H_2 + H, and C_2H_2 + CH, while the C_3H_2 produces C_3 + H_2, C_2H + CH, and C_2H_2 + C. The translational energy distributions for each one of these steps have been derived using the forward convolution technique. These energy distributions reveal the exit barriers and other constraints on the potential energy surfaces that lead to the above stated products.

Introduction

There have been many studies of the geometrical isomerization of the C_3H_4 molecule since conversion among the various forms of the molecule exhibits most of the behavior that is important in its chemistry [1,2,3]. On the ground state surface there are pathways involving 1,3 and successive 1,2 H migration that can convert the molecule from propyne to allene. The hydrogen migration step can also be followed by a ring closure step that can convert allene or propyne to cyclopropene. Theoretical calculations have shown that there are large activation energy barriers of the order of 60 kcal/mole between the various geometrical isomers [3]. These barriers are significantly lower than the energy required for dissociation from the ground electronic state (~ 100 kcal/mol) so that the possibility exsist for extensive isomerization prior to dissociation. Infrared multiphoton excitation, (IRMPE), studies in the bulk gas support these calculations since they show that the principal product from the IRMPE of allene is propyne [4]. Shock tube measurements of this isomerization reaction yield an activation energy of 60 kcal/mole which also agrees with these theoretical calculations [5].

Ultraviolet photochemistry of the S_1 and S_2 electronic states often occurs via internal conversion of these excited states to the vibrational continuum of the ground state where dissociation takes place. Thus photoexcitation can be used as a pathway for the production of highly vibrationally excited molecules in the ground electronic states, whose energy is determined by the wavelength of the exciting light. If internal conversion of electronically excited molecules is fast, and the highly vibrationally excited molecules live long enough, then all of the geometrical isomers may exhibit similar dynamics since they are well above all energy barriers to the various isomeric forms.

The radicals that can be formed in the primary and secondary photolysis of allene are important in understanding soot formation in combustion, C_3 formation in comets, and the presence of cyclopropenylidiene which is currently thought to be the most abundant hydrocarbon in interstellar space [6, 7, 8, 9]. Thus, the more we understand about the

secondary photolysis of the radicals produced in the initial photolysis of allene, the better we will be able to understand these areas.

Finally, understanding the individual photochemical processes, especially when they occur on the ground state potential surface, will also help us to understand the reverse chemical reactions which are often difficult to study in the laboratory. For example, it will be shown that one of the primary photolytic steps is the production of H_2 and singlet C_3H_2. Studying the reverse reaction of H_2 and C_3H_2 in the laboratory, even if it did occur on the ground state surface, would be difficult because a clean source of C_3H_2 would be needed and the reactants would have to collide at relatively high translational or vibrational energies to overcome the barriers involved in the reaction.

Experimental

The angle resolved time of flight(TOF) experiments were performed using two different molecular beam machines. One of these machines is a rotating source machine with a fixed detector (hereafter called RS) which was designed specifically for photochemical studies and has been previously described [10]. In this machine a continuous molecular beam is crossed at 90° with the output of a pulsed ArF laser. TOF spectra of the products of photodissociaton are measured using a mass spectrometer consisting of an electron impact ionizer, a quadrupole mass filter and an ion counting detector. The molecular beam source may be rotated about the axis defined by the path of the laser beam in order to collect time of flight spectra at different molecular beam - detector angles. The other machine which is used for measuring H and H_2 products is equipped with a pulsed molecular beam with a 35" diameter rotating detector (hereafter called the RD machine) which was specially configured for crossed molecular beams studies of D + H_2. It also has been previously described [11]. The basic concept of the experiment is illustrated by the Newton diagram in Fig. 1 for the photodissociation reaction,

$$C_3H_4 + h\nu_{193nm} \rightarrow C_3H_2 + H_2 \qquad (1)$$

The beam is moving with a velocity, v_{beam}, in the laboratory reference frame, but in the center-of-mass(CM) frame the C_3H_4 molecules are at rest. Conservation of linear momentum requires that the linear momentum of C_3H_2 is equal to that of H_2 in the CM frame. The radii of the circles in this diagram correspond to the recoil velocities in the CM frame and represent the maximum translational energy released in the reaction as determined by the analysis discussed below. The experiment, however, measures the velocity in the laboratory frame, at a particular laboratory molecular beam - detector angle. This velocity is the resultant between the beam velocity, and the recoil velocity in the CM frame at that observation angle. In some cases the velocity is uniquely determined at a particular laboratory angle but in other cases, as Fig. 1 shows, one can observe fragments that are both forward and backward scattered in the CM frame with respect to the direction of the molecular beam. By determining the TOF spectra at different angles one can obtain the distributions of recoil velocities of the fragments in the CM frame using a forward convolution technique which averages an assumed CM distribution over the velocity distribution in the molecular beam and the instrumental resolution [12].

The CM recoil velocity can be used to determine an overall energy balance for the photochemical reaction, which is given for reaction 1 by,

$$E_{int} = h\nu_{193nm} - \Delta H(1) - E_{Trans} \qquad (2)$$

In this equation, ΔH is the enthalpy of the reaction in the absence of the light, E_{int} is the internal excitation of the fragments and E_{Trans} is the total translational energy which is the sum of the translational energies of the fragments. In principle one only needs to determine the recoil velocity of one of the fragments since the velocity of the other fragment may be calculated using conservation of linear momentum. In practice, it is better to measure the recoil velocities of both fragments at several angles to provide additional data to test the proposed reaction mechanism.

The fragments are detected by electron impact ionization using 200 eV electrons, mass selected and counted as ions. A large amount of dissociative ionization was observed for many products and it is necessary to deconvolute ion signals from various products which yield the

same daughter ions. For example, part of the signal observed at a lower mass-to-charge ratio (m/e) may contain a fragment ion from a higher mass peak. Again this can be accounted for by carefully comparing features which appear in the TOF spectra monitored at various mass numbers at different laboratory angles.

The experiments using the RS machine were all done at 193 nm using a Lambda Physik EMG 103 ILC laser. The output of this laser was usually 70 mJ in a 28 ns pulse and it was focused to a 3 mm by 1 mm spot at the interaction region. This yields a peak laser intensity of about 8 x 10^{25} photons $cm^{-2}s^{-1}$ at the interaction region. One experiment was done with 248 nm but only a weak photolysis signal could be observed.

In the RS machine a continuous supersonic beam was formed by expanding 120 torr of a mixture consisting of 6% allene in He through a 0.125 mm diameter nozzle heated to 150°C. Under these conditions no signal at m/e = 40, ($C_3H_4^+$), was observed at a laboratory angle of 7 degrees from the beam, indicating that the photodissociation of clusters was not occurring under these circumstances. He was used as a carrier gas since it increases the average velocity of the beam, enhancing the observed signal by confining the products to a smaller forward cone about the direction of molecular beam.

A Lambda Physik EMG 202 MSC ILC laser operating at 193 nm was used with the RD machine. This laser can supply higher pulse energies of the order of 150 mJ per pulse. To compensate for the higher pulse energies of this laser it was only focused to a 3mm by 3 mm area so that the intensity in the interaction region was similar to that on the RS machine. The pulsed molecular beam was formed by expansion of 40 torr of pure allene through a 1 mm nozzle.

The allene was obtained from Matheson and used without further purification. No evidence was found that the 1.2% of propyne and propylene impurities which are present in the gas caused any problems in the present experiments. The biggest of these impurities is propyne (0.7 %) whose absorption coefficient of 1.2 x 10^{-18} cm^2 is twice as large as the absorption

coefficient of allene which is 0.6 x $10^{-18}cm^2$ [13, 14]. Thus, less than 1.4% of the observed fragments could come from propyne.

Results and Discussion

Fragments containing three carbon atoms, C_3H_n

The C_3H_n(n = 3,2,1, or 0) fragments all must come from the elimination of H or H_2 in primary or secondary photodissociation steps. The TOF spectra obtained at 7° and 10° for m/e = 39, $C_3H_3^+$, is shown in Fig. 2. The solid line is a forward convolution fit to the data points using the $P(E_T)_{39,1}$ shown in Fig. 3 [15]. The notation $P_{i,j}(E_T)$ stands for a translational energy distribution for the A (mass = i + j) + hν → B(mass = i) + C(mass = j). The appearance of m/e = 39 at 7° and 10° where no m/e = 40 is observed proves reaction 3 is one of the primary processes in the photodissociation of allene,

$$C_3H_4 + h\nu \rightarrow C_3H_3 + H \qquad (3).$$

No signal at m/e = 39 was observed at 20° or 30° so signals observed at lower masses at these wider angles must come from other channels. Signal from a second channel is observed at m/e = 38 at 20° as shown in Fig. 5. No signal at m/e = 38 was observed at 30° but a signal is observed at m/e = 37 and 36 at 30° as shown in Figs. 7 and 9 . These fragments must also come from new channels that are not present at m/e = 39 and 38. The data analysis consists of quantitatively fitting these TOF spectra using the forward convolution technique by using a trial translational energy distribution, $P(E_T)$, for each assumed process and requiring that the same $P(E_T)$ also fits the TOF spectrum of the other recoil fragment, as required by conservation of linear momentum.

The $P(E_T)_{39,1}$ which fits the data in Fig. 2 is given in Fig. 3. It is a curve that peaks at a translational energy, E_T, of 3.9 kcal/mole and then decreases, cutting off at an $E_T(max)_{39,1}$ = 36.4 kcal/mol. The low energy part of this curve was determined from the fit, to the slow part of the H atom TOF spectrum, shown in Fig. 4, which is very sensitive to the slow part of the $P(E_T)$. The high energy part of this $P(E_T)$ was most sensitive to the fast part of the m/e = 39 TOF spectra at 7 and 10 degrees, which illustrates the advantage of determining both recoil

fragments since different parts of the $P(E_T)$ may be sensitive to different parts of the TOF spectra for the corresponding fragments. The shape of the $P(E_T)$ is consistent with a model in which internal conversion produces a vibrationally excited molecule which undergoes simple bond rupture with no appreciable exit barrier.

The upper bound of the C-H bond dissociation energy, $D_0(C\text{-}H)_{39,1}$, for allene can be derived from the above data using the following equation,

$$D_0(C\text{-}H)_{39,1} \leq h\nu - E_T(max)_{39,1} \quad (4)$$
$$\leq 111.7 \text{ kcal/mol}$$

This upper bound is considerably higher than the bond dissociation energy one would compute from the best estimated $\Delta H_{f,0}^0$ of Melius for H, C_3H_3 and C_3H_4 [16,17]. The $\Delta H_{f,0}^0$ from Melius, which are used for consistency throughout this paper, yields a bond dissociation energy of only 85.6 kcal/mol [16]. Thus, the experimental observations suggest that the C_3H_3 radical is formed with a minimum internal energy of 26.1 kcal/mol. This minimum internal energy could be in the form of vibrational, rotational, or electronic energy. The presence of excess vibrational energy is in agreement with recent observations of transient IR emission from this system [18]. It is unlikely the radical is formed electronically excited because recent theoretical calculations show that the first excited doublet state is about 79 kcal/mole above the ground state [19]. It is generally agreed that the most stable form of the C_3H_3 radical is the propargyl form of the radical [17] but there are a variety of isomeric forms of this radical and the experimental results could be interpreted to mean that there is a difference of at least 26.1 kcal/mol between the initially formed C_3H_3 radical and the ground state of the propargyl radical. Ab-initio calculations of the energies of C_3H_3 and indirect experimental measurements have both suggested that there are however no additional barriers between the various isomeric forms of the radical aside from the differences in heat of formations [20]. The allenyl form of the radical was found to have an energy 61 kcal/mol higher than the propargyl radical. The C_3H_3 radical is probably formed with an excess amount of vibrational energy because of the rearrangement the radical undergoes after it releases the H atom. The average energy released

in translational motion for this channel is 8.95 kcal/mole which is much lower than the maximum translational energy. Thus the average internal energy of the C_3H_3 radicals formed in reaction 3 is about 53.6 kcal/mole, which is still not enough energy to electronically excite the radical [19]. Therefore all of the internal energy must be in the vibrational and rotational motion of the C_3H_3 radical. Because of the low mass of the H atom, it is unlikely that much rotational energy is imparted to C_3H_3 as it leaves the reaction center so that most of this excess energy should be in vibrational motion.

The TOF spectrum of m/e = 38 ($C_3H_2^+$) at 7°, 10° and 20° is shown in Fig. 5. The largest contribution to the m/e = 38 ($C_3H_2^+$) peak at 10° is due to the C_3H_3 + H channel. In fact the contribution of reaction (1) at m/e = 38 is larger than the total count rate at mass 39. This is a reflection of the large amount of internal energy present in the C_3H_3 radical when it reaches the ionizer, which significantly increases the probability for dissociative ionization and is in complete accord with our earlier conclusion that the C_3H_3 product must be highly vibrationally excited. At 10° a small percentage of the fast m/e = 38 fragments could not be accounted for by the C_3H_3 + H channel. This additional signal could be due to a C_3H_2 + H_2 primary photochemical process or a C_3H_2 + H secondary photochemical process. All of the signal at 20° must come from one or both of these channels since no m/e = 39 signal is seen at this angle. The fit shown in Fig. 5 is in fact a fit with both of these channels and the $P(E_T)$'s used to fit the experimental observations are given in Figs. 3 and 6. At a detection angle of 20°, 93% of the signal is due to the secondary photolysis of the C_3H_3 via the following reaction,

$$C_3H_3 + h\nu \rightarrow C_3H_2 + H \qquad (5)$$

This simple bond rupture reaction has a $P(E_T)_{38,1}$ that is similar in its appearance to the $P(E_T)_{39,1}$ obtained from the primary reaction channel.

Only 7% of the signal at mass 38 is due to the second primary channel,

$$C_3H_4 + h\nu \rightarrow C_3H_2 + H_2 \qquad (6)$$

The shape of $P(E_T)_{38,2}$ suggests that there is an exit barrier exceeding 20 kcal/mol for the $C_3H_2 + H_2$ channel which is in accord with our expectations for a molecular dissociation channel.

There is a small signal in the m/e = 37 (C_3H^+) TOF spectra at 30° which is shown in Fig. 7. This is a clear indication that new channels have to be added to the dissociation scheme. The solid curve in this figure is a fit to the data adding an additional secondary channel from C_3H_3,

$$C_3H_3 + h\nu \rightarrow C_3H + H_2 \qquad (7)$$

At the smaller angles of 10° and 20° the contributions from the other channels that were present at higher masses tend to dominate the fit.

The TOF spectra for m/e = 36 (C_3^+) are shown in Fig. 8 at 10°, 20°, and 30°. The fast part of the TOF curve at 30° can not be fit with the above dissociation channels and a new channel has to be added. The only secondary channel that would not involve three photons but still form C_3 is,

$$C_3H_2 + h\nu \rightarrow C_3 + H_2 \qquad (8)$$

Recently, laser induced fluorescence detection of the C_3 radical formed by 193 nm photolysis of a pulsed molecular beam of allene has confirmed that this radical is produced [21]. Payne and Stief have also presented evidence that C_3 is formed by the one photon sequential detachment of two H_2 molecules in the 123.6 nm photolysis of propyne [22]. It is therefore not surprising that there is a two photon channel which results in the sequential detachment of H_2 in the 193 nm laser photolysis of allene since it is a geometrical isomer of propyne and the energy of the first of these photons should be high above any geometrical barriers. The energy of two photons at 193 nm is also 2.8 eV higher than the energy of a single 123.6 nm photon. It is likely that the C_3H_2 radical has some internal excitation energy when it is formed. Absorption of a second 193 nm photon should supply enough energy to allow facile hydrogen atom migration over any internal barriers that may be present on the potential energy surface and form H_2 [1]. The shape of $P(E_T)_{36,2}$ suggests that there is an exit barrier of at least 33 kcal/mol for the $C_3 + H_2$ channel.

H and H_2 Products

All of the C_3H_n channels produce either hydrogen atoms or hydrogen molecules, so that the $P(E_T)$ that have been derived from the fit of the TOF data for the C_3H_n masses should also fit the TOF data obtained for H and H_2. Fig. 4 shows that this is the case, which indicates that these $P(E_T)$'s satisfy the required momentum constraints.

If the dissociation processes only involved the elimination of H and H_2, with C_3 being the smallest C-containing product,then the TOF spectra of all of the masses below mass 36 would be able to be fit with these same $P(E_T)$'s used to fit the C_3H_x, H, and H_2 channels. But, since large amounts of vibrational energy are probably retained in the C_3H_3 and C_3H_2 fragments when they are formed, it is likely, as will be shown below, that other secondary processes not involving H atoms are also present.

The C_2H_n and CH_n Fragments

The TOF spectra for the C_2H_n (n=3,2,1,0) fragments are shown in Figs. 9, 11 and 12. Comparisons of these TOF curves with the earlier curves at the same angles but higher masses show that there is additional signal at shorter times for the C_2 fragments and additional dissociation channels are needed to fit these spectra.

To fit the fast part of the TOF spectrum for m/e = 26 ($C_2H_2^+$), shown in Fig. 9, a new secondary channel had to be added. This channel is the production of C_2H_2 and CH via the following process,

$$C_3H_3 + h\nu \rightarrow C_2H_2 + CH \quad (9)$$

This secondary channel requires only two photons and results in the secondary dissociation of the principal radical fragment. A second two photon channel involving the C_3H_2 radical can also be invoked to explain part of the fast part of the TOF curves at m/e = 25, 24, and 13 (C_2H^+, C_2^+ and CH^+).

$$C_3H_2 + h\nu \rightarrow C_2H + CH \quad (10).$$

The contributions of reaction 9 and 10 to the TOF curves for m/e = 25, 24, 13, and 12 are almost indistinguishable from each other. However, in view of the fact that m/e = 26 has a count rate higher than the other masses in this region it is likely that reaction 9 is the dominant C-C bond rupture channel. Neither of these channels account for the fast part of m/e = 12 (C^+), so a third secondary channel has to be invoked. This third channel is the dissociation of the C_3H_2 radical via,

$$C_3H_2 + h\nu \rightarrow C_2H_2 + C(^3P) \qquad (11)$$

The carbon atom has to be in the (^3P) state so that enough translational energy is available to fit the fast part of the m/e = 12 peak. The presence of a spin forbidden process can be rationalized on the basis that the C_3H_2 is produced with enough internal energy to promote intersystem crossing. The contribution of this channel is much smaller than reaction 9 because this is secondary dissociation of a minor primary product.

There are many isomeric forms of the C_3H_3 and the C_3H_2 radicals and with the amount of internal energy that is left in the C_3H_3 and the C_3H_2 a lot of these are probably accessible at the energies used in our study [19,20,23,24,25,26,27]. A likely transition state for reaction 9 is a cyclic form of the C_3H_3 radical [20]. A prop-2-ynylidene type transition state could easily explain reaction 10 [24]. The minor primary process eliminates molecular H_2 and should leave a C_3H_2 radical that is colder than the C_3H_3 radical because some of the available energy is carried away by the fast vibrationally excited H_2 product. The C_2H_2 product from C_3H_2 suggest that the secondary dissociation reaction 11 goes through either a linear propadienylidene or a cyclic transition state [24]. The propadienylidene form of the C_3H_2 radical could be formed by 1,1-H_2 elimination which then is electronically excited via absorption of a second 193 nm photon and dissociates to produce C_2H_2 + C. Calculations show the propadienylidene C_3H_2 radical has a minimum which lies 14.5 kcal/mole [25] above the minimum of the lowest geometrical isomer of C_3H_2, the cyclopropenylidene radical [24]. This is well within the exothermicity of reaction 6. The cyclic form of the C_3H_2 could be formed after dissociation of C_3H_4. To explain the formation of $C(^3P)$ by either mechanism the C_3H_2 would then have to

undergo intersystem crossing either before or after absorption of the second photon. More definitive experiments, perhaps starting with a beam of cold radicals, will be required to confirm the details of the secondary dissociation dynamics.

Branching Ratios

The complexity of the observed reaction mechanism makes it difficult to calculate branching ratios from the fits to the fragment TOF curves below m/e= 36. There is not enough structure in the observed TOF curves to unambiguously assign the relative contributions at these lower masses. The situation is different, however, for the primary and secondary channels that produce H and H_2. The fits at the various angles and at high and low masses are very sensitive not only to the shapes and energies for the $P(E_T)$'s but also to the relative contribution of each channel to the TOF spectrum. Once the shapes and energies have been determined by fitting all of the data for the H, H_2 and C_3H_n fragments, then the total number of counts for the H and H_2 channels may be used to calculate the branching ratios for the primary and secondary channels. Of course the ratio of the primary to the secondary channel has to be fluence dependent because the secondary channels are two photon processes.

The total number of counts at m/e= 1 is 6 times larger than the count rate for m/e= 2. Since the lab velocities of H and H_2 are much higher than the heavier C-containing fragments no higher masses interfere with either one of these TOF spectra. All of the m/e = 1 signal comes from either Reaction 3 or Reaction 5, so that it represents almost the total amount of C_3H_3 formed. A very small amount of C_3H_3 dissociates to form C_3H and H_2 so that some of the C_3H_3 radicals contribute to this signal. The total count rates found for each of the channels used to fit the m/e = 1 and 2 may be used along with the relative ionization cross sections at 200 eV to calculate the primary quantum yields for the formation of H and H_2 at 193 nm [28]. This data and the results of the calculations are collected in Table 1. The results in this table show that the branching ratio for H atom elimination to H_2 elimination is 0.89:0.11. The secondary branching ratio for H and H_2 elimination from the photolysis of vibrationally excited

C_3H_3 radicals is 0.94:0.04. In both cases, i.e. primary and secondary photolysis, the molecular elimination channel is considerably smaller than the atom elimination channel.

Conclusions

The photodissociation of allene has been studied at 193 nm and the two primary and six secondary processes that have been identified are summarized in Fig. 14. Most of the dissociation pathways involve H_2 or H atom elimination, with H atom elimination being the most prevalent. The major primary process is the formation of vibrationally excited C_3H_3 by H atom elimination. The observed translational energy for this process suggests the minimum amount of vibrational energy that must be in this radical is 26.1 kcal/mole since ab-initio calculations say there is no stable electronic state at or near this energy [19]. The form of the translational energy distribution curve is consistent with the formation of the C_3H_3 radical via unimolecular decomposition of highly excited ground state C_3H_4. If there is no exit barrier this kind of decomposition leads to a translational energy distribution that peaks at low translational energies and then monotonicaly decreases to the thermodynamic limit [29,30]. It also implies that randomization of the available energy in the excited C_3H_4 molecule occurs before fragmentation. The other primary process produces internally excited C_3H_2 by H_2 elimination, though the C_3H_2 is probably not as excited as the C_3H_3 radical because some of the available energy should be used for vibrational excitation of the H_2 fragment. The highly excited hydrocarbon radicals produced in the primary processes lead to a variety of products when they absorb a second photon. The type of products that are observed are in accord with the many different geometrical forms that are possible for the C_3H_3 and C_3H_2[20, 25, 27].

Acknowledgements

William M. Jackson would like to acknowledge the Miller Foundation and the Guggenheim Foundation for their support when much of this work was done. He would also like to acknowledge the support the National Science Foundation for his summer salary under Grant number CHE-9008095 when the analysis of the data was finished and the paper written. Some of his work on this paper was also supported by the DOE Combustion program of Basic Energy Science under grant # DE-FG05-84er-13213. This work was also supported by the Director, Office of Energy Research, Office of Basic Energy Sciences, Chemical Sciences Division of the U. S. Department of Energy under contract # DE-AC03-76SF00098.

Table 1

Primary and Secondary Signal Counts

for the H and H_2 peaks at a 90° detection angle

	Reaction	Total Number of Counts	Relative Yields
Primary	$C_3H_4 \rightarrow C_3H_3 + H$	83,967	0.81
	$C_3H_4 \rightarrow C_3H_2 + H_2$	19,430	0.19
Secondary	$C_3H_3 \rightarrow C_3H_2 + H$	108,543	0.96
	$C_3H_3 \rightarrow C_3 + H_2$	4,163	0.04
	$C_3H_2 \rightarrow C_3 + H_2$	2,289	--

The total number of counts in this table has been corrected for the number of laser shots and the relative ionization cross section of H and H_2. No correction was made for the difference in the velocities of H and H_2. The Laser fluence was 2.5 J/cm^2.

1. N. Honjou, J. Pacansky, and M. Yoshimine, J. Am. Chem. Soc., 107, 5332(1985).

2. M. Yoshimine, J. Pacansky, and N. Honjou, J. Am. Chem. Soc., 111, 2785(1989).

3. M. Yoshimine, J. Pacansky, and N. Honjou, J. Am. Chem. Soc., 111, 4198(1989)

4. M. L. Lesiecki, K. W. Hicks, A. Orenstein, and W. A. Guillory, Chem. Phys. Lett. 71, 72(1980).

5. A. Lifshitz, M. Frenklach, and A. Burcat, J. Phys. Chem. 79, 1148(1975).

6. I. R. Slagle and D. Gutman, Twenty-first Symposium (International) on Combustion, The Combustion Institute, 875(1986).

7. P. Thaddeus, J. M. Vrtilek, and C. A. Gottlieb, Astrophys. J. 299, L63(1985).

8. B. G. Marsden, Ann. Rev. of Astron. and Astrophys., 'Comets', 12, 1(1974).

9. W. M. Jackson, 'Laboratory studies of photochemical and spectroscopic phenomena related to comets', L. L. Wilkening, Ed. University of Arizona Press, 480(1982).

10. A. M. Wodtke and Y. T. Lee, 'High Resolution Photofragmentation Translational Spectroscopy, in Advances in Gas-Phase Photochemistry and Kinetics, Molecular Photodissociation Dynamics, M. N. R. Ashfold and J. E. Baggott, Eds. Royal Society of London, p. 31 (1987).

11. R.E. Continetti, B.A. Balko, and Y.T. Lee, J. Chem. Phys. 93, 5719, (1990).

12. Xinsheng Zhao, "Photodissociation of cyclic compounds in a molecular Beam', Lawrence Berkeley Laboratory Report, LBL-26332(1988).

13. T. K. Nakayama and K. Watanabe, J. Chem. Phys., 40, 558(1964).

14. K. Fuke and O. Schnepp, Chem. Phys.,38, 211(1979).

15. Throughout the text the notation $N_{x,y}$ will be used to denote a reaction step A (mass = x+y) + $h\nu \rightarrow$ B (mass = x) + C (mass = y).

16. Carl Melius, Sandia National Laboratory, Private communication.

17. D. F. McMillen and D. M. Golden, Ann. Rev. Phys. Chem. 33, 493(1982).

18. W.M. Jackson, Rong Rong Zhu, Mansour Zahedi, and Fida Mohammad, unpublished results.

19. H. Honjou, M. Yoshimine and J. Pacansky, J. Phys. Chem., 91, 4455(1987).

20. G. Collin, H. Deslauriers, G. R. DeMare, R. A. Poirier, J. Phys. Chem., 94, 134(1990).

21. Yihan Bao, Randy Urdahl, Xueyu Song and W.M. Jackson, unpublished results.

22. W. A. Payne and L. J. Stief, J. Chem. Phys., 56, 3333 (1972).

23. G. Maier, H. P. Reisenauer, W. Schwab, P. Carsky, B. A. Hess, Jr., L. J. Schaad, J. Am. Chem. Soc., 109, 5183(1987).

24. G. Maier, H. P. Reisenauer, W. Schwab, P. Carsky, V. Spirko, B. A. Hess, Jr., L. J. Schaad, J. Chem. Phys., 91, 4763, (1989).

25. D. J. DeFrees, A. D. McLean, Ap. J., 308, L31(1986).

26. D.L. Cooper, and S. C. Murphy, Ap. J., 333, 482(1988).

27. T. J. Lee, A. Bunge, H. F. Schaefer III, 107, 137(1985).

28. L. J. Kieffer, Compilation of Low Energy Electron Collision Cross Section Data:Part 1, JILA Report #6, (1969).

29. A. M. Wodtke, E. J. Hinsta and Y. T. Lee, J. Phys. Chem. 90, 3549(1986).

30. S. A. Safron, N. D. Weinstein, D. R. Herschbach, J. C.Tully, Chem. Phys. Lett. 12, 564(1972).

Figure Captions

Fig. 1. Newton Diagrams for the Primary Photodissociation channels in the photolysis of allene at 193 nm.

Fig. 2. Time of Flight spectra for m/e = 39 at 7 and 10 degrees. The points are data and the solid line is the fit obtained using the forward convolution technique. The translational energy distribution used for this fit is shown in Fig. 3. The data are normalized (as in all the figures) to 10^4 laser shots.

Fig. 3. Translational energy distribution curves, $P(E_T)$, for the two primary processes, reaction 3 and 6, in the allene photodissociation at 193 nm. These were used to fit the time of flight data shown in Figs. 2 and 5.

Fig. 4. Time of flight spectra for m/e = 1 and 2 taken with the RD machine. The solid line through the points represent the total fit made of the following components: In the m/e = 1 data, Reaction 3(-·-·, dash-dot) and Reaction 5 (---, dash); in the m/e = 2 data, Reaction 6 (-·-·, dash-dot), Reaction 7 (---, dash), and Reaction 8 (-, solid).

Fig. 5. Time of Flight spectra for m/e 38 at 7, 10 and 20 degrees. The points are data and the solid line is the fit obtained using the forward convolution technique. The translational energy distribution used for this fit is shown in Fig. 3. The components first appearing at this m/e are due to Reaction 6 (-·-·, dash-dot) and Reaction 5 (---, dash). The daughter ion of the Reaction 3 product formed by fragmentation in the ionizer is given by a solid lines.

Fig. 6. Translational energy distribution, $P(E_T)$, for the secondary photochemical processes that produce H or H_2 products in the allene photodissociation at 193 nm. These were used to fit the time of flight data shown in Figs. 4, 6, 7, 8, 10, 11, and 12.

Fig. 7. Time of flight spectra for m/e = 37 at 10 20 and 30 degrees. The points are data and the solid is the fit obtained with the $P(E_T)$'s shown in Figs. 3 and 5. The component first appearing at this m/e is due to Reaction 7 (---, dash). Components due to the daughter ions of other reactions (identified at higher m/e) formed by fragmentation in the ionizer appear as solid lines.

Fig. 8. Time of flight spectra for m/e = 36 at 10, 20 and 30 degrees. The points are data and the solid line is the fit obtained with the $P(E_T)$'s shown in Figs. 3 and 5. The component first appearing at this m/e is due to Reaction 8 (---, dash). Components due to the daughter ions of other reactions (identified at higher m/e) formed by fragmentation in the ionizer appear as solid lines.

Fig. 9. Time of flight spectra for m/e = 26 at 7, 10, and 20 degrees. The points are data and the fit obtained with the $P(E_T)$'s shown in Figs. 3, 5, and 9. The components first appearing at this m/e are due to Reaction 9 (---, dash) and Reaction 11 (-·-·, dash-dot). Components due to the daughter ions of other reactions (identified at higher m/e) formed by fragmentation in the ionizer appear as solid lines.

Fig.10. Translational energy distributions curves for non-hydrogen producing secondary channels.

Fig.11. Time of flight spectra for m/e = 25 at 7, 10, 20 and 30 degrees. The points are data and the solid line is the fit obtained with the $P(E_T)$'s shown in Figs. 3, 5, and 9. The component first appearing at this m/e is due to Reaction 10 (---, dash) and makes a small contribution. Components due to the daughter ions of

other reactions (identified at higher m/e) formed by fragmentation in the ionizer appear as solid lines.

Fig.12. Time of flight spectra for m/e = 24 at 20 and 30 degrees. The points are data and the solid line is the fit obtained with the $P(E_T)$'s shown in Figs. 3, 5, and 9. Reaction 10 is indicated by (---, dash). Components due to the daughter ions of other reactions (identified at higher m/e) formed by fragmentation in the ionizer appear as solid lines.

Fig.13. Time of flight spectra for m/e = 12 and 13 at 10 degrees. The points are data and the solid line is the fit obtained with the $P(E_T)$'s shown in Figs. 3, 5, and 9. The following components are indicated : In the m/e = 13 data, Reaction 10 (---, dash) and Reaction 9 (-·-·, dash-dot): in the m/e =12 data Reaction 10 (---, dash), Reaction 9 (-·-·, dash-dot) and Reaction 11 (-··-··, dash-dot-dot). Components due to daughter ions of reaction products identified at higher m/e appear as solid lines.

Fig.14 Schematic of Proposed Dissociation Mechanism

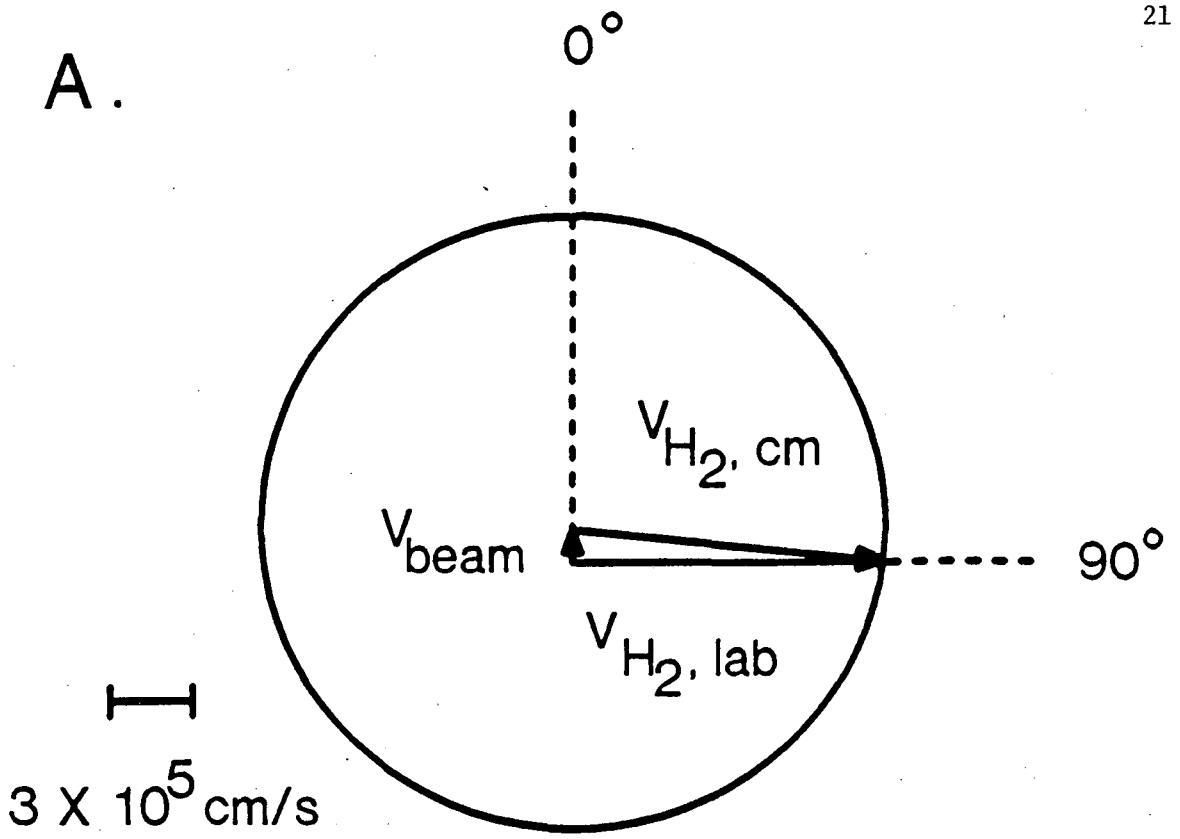
A.
0°
$V_{H_2, cm}$
V_{beam}
90°
$V_{H_2, lab}$
3×10^5 cm/s

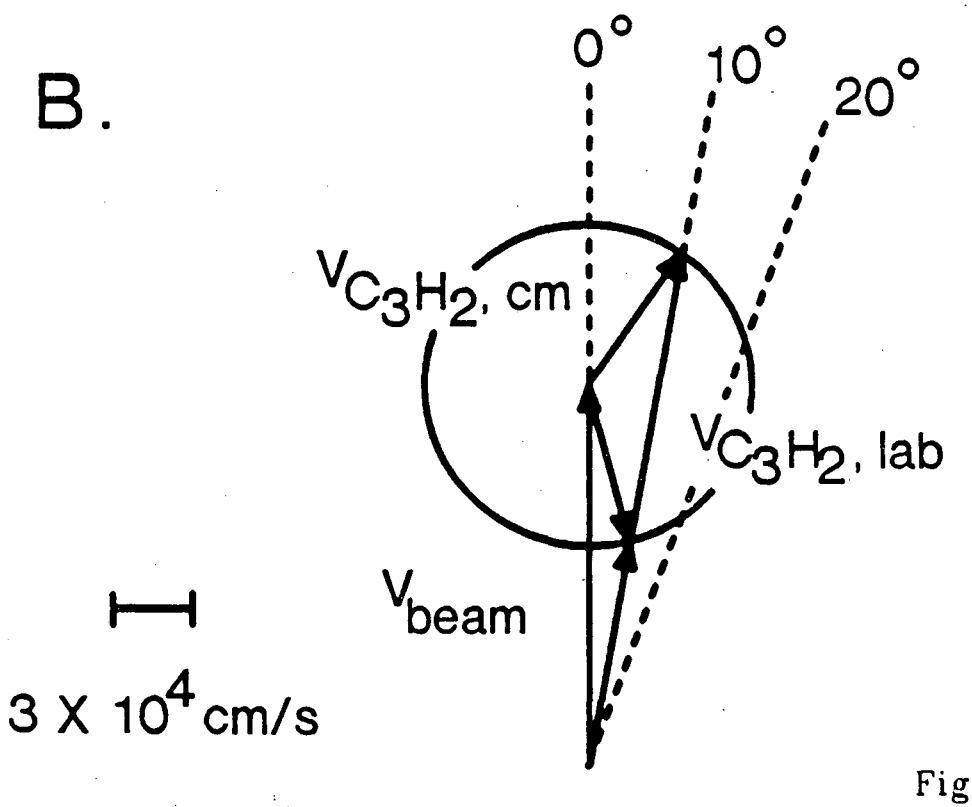
B.
0°
10°
20°
$V_{C_3H_2, cm}$
$V_{C_3H_2, lab}$
V_{beam}
3×10^4 cm/s

Fig. 1

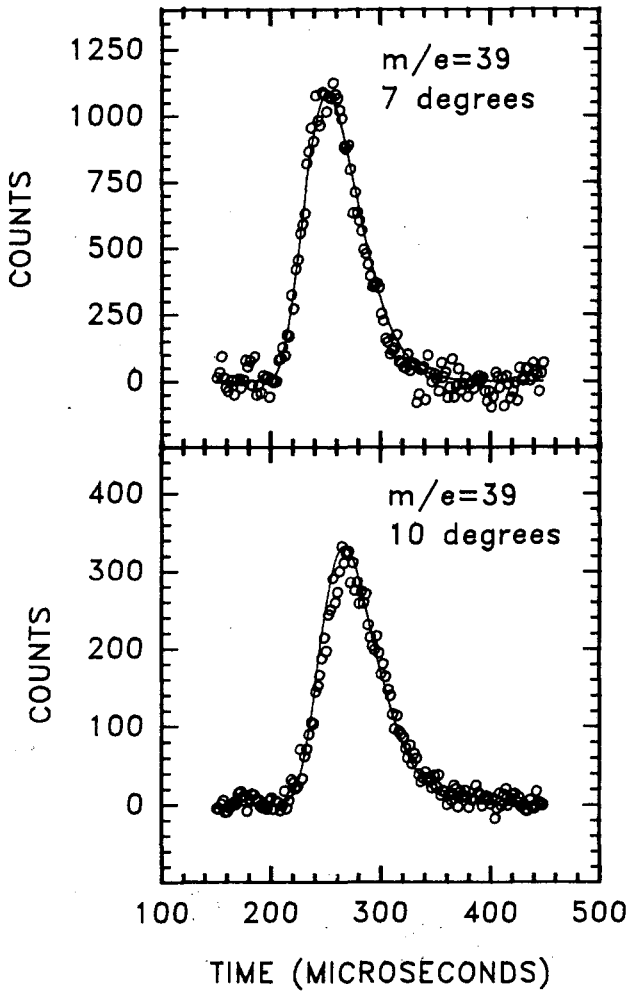
m/e=39
7 degrees
COUNTS
1250
1000
750
500
250
0
m/e=39
10 degrees
COUNTS
400
300
200
100
0
100
200
300
400
500
TIME (MICROSECONDS)

Fig. 2

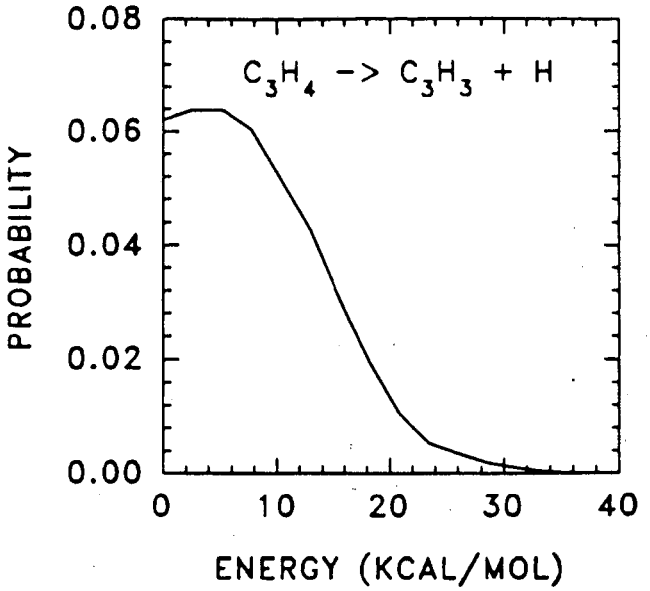
0.08
0.06
0.04
0.02
0.00
PROBABILITY
C_3H_4 -> C_3H_3 + H
0
10
20
30
40
ENERGY (KCAL/MOL)

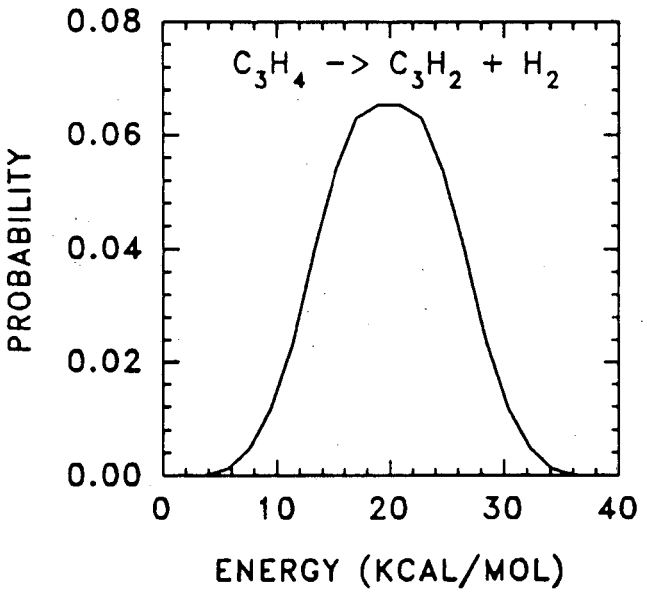
0.08
0.06
0.04
0.02
0.00
PROBABILITY
C_3H_4 -> C_3H_2 + H_2
0
10
20
30
40
ENERGY (KCAL/MOL)

Fig. 3

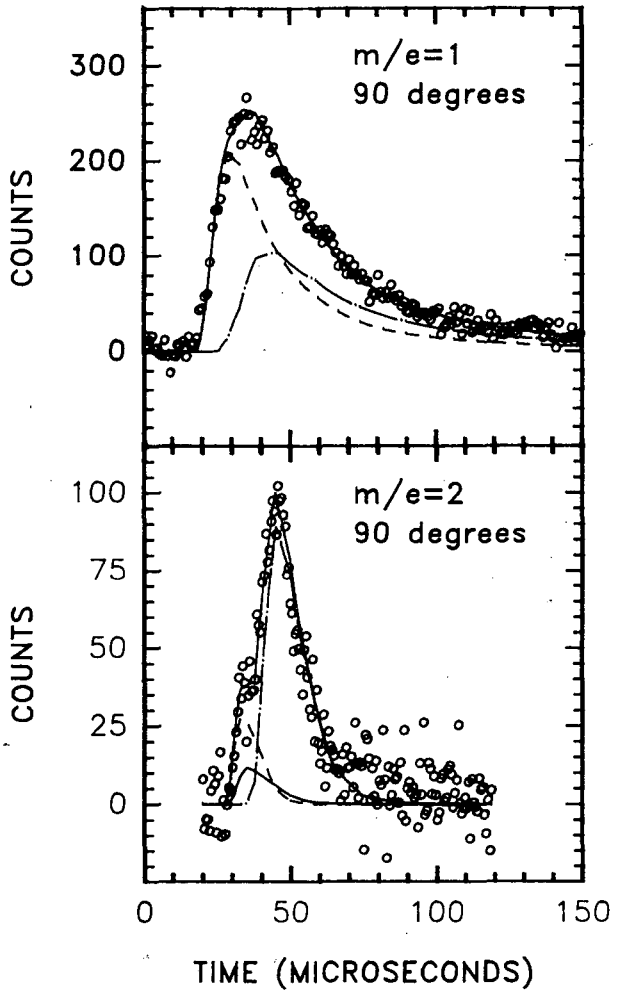
m/e=1
90 degrees
COUNTS
300
200
100
0
m/e=2
90 degrees
COUNTS
100
75
50
25
0
0
50
100
150
TIME (MICROSECONDS)

Fig. 4

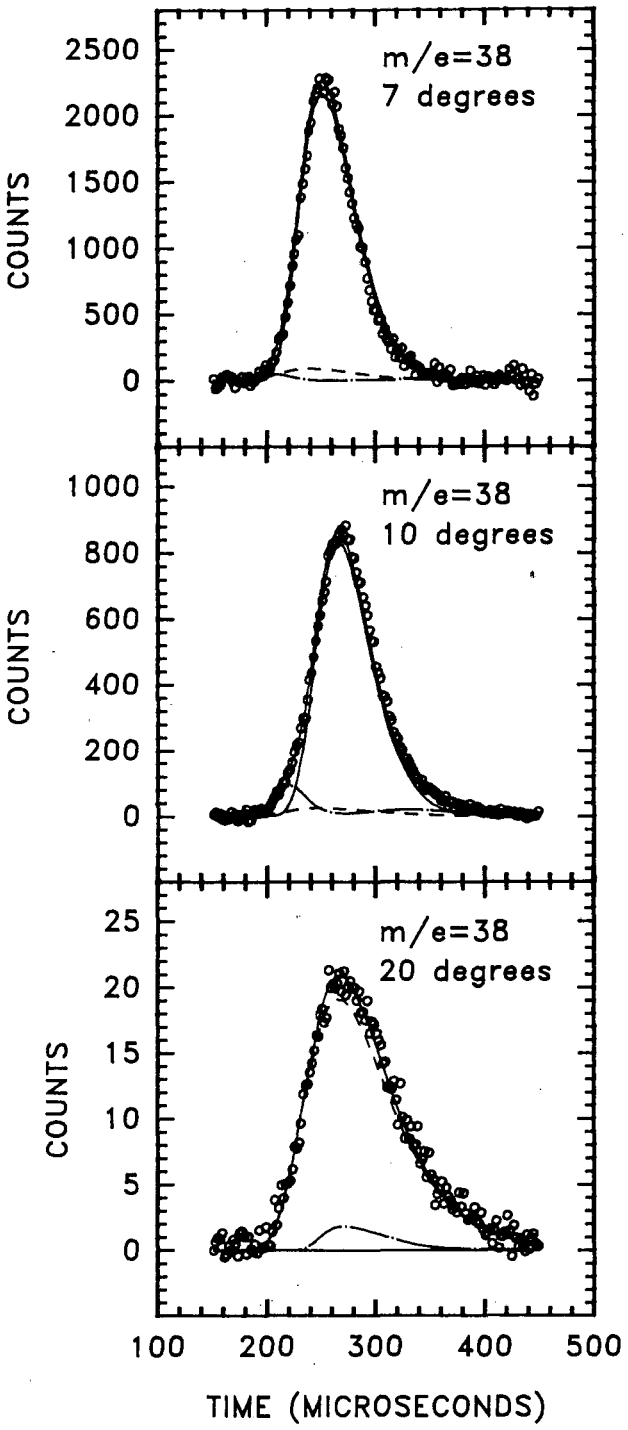
m/e=38
7 degrees
m/e=38
10 degrees
m/e=38
20 degrees
COUNTS
COUNTS
COUNTS
2500
2000
1500
1000
500
0
1000
800
600
400
200
0
25
20
15
10
5
0
100
200
300
400
500
TIME (MICROSECONDS)

Fig. 5

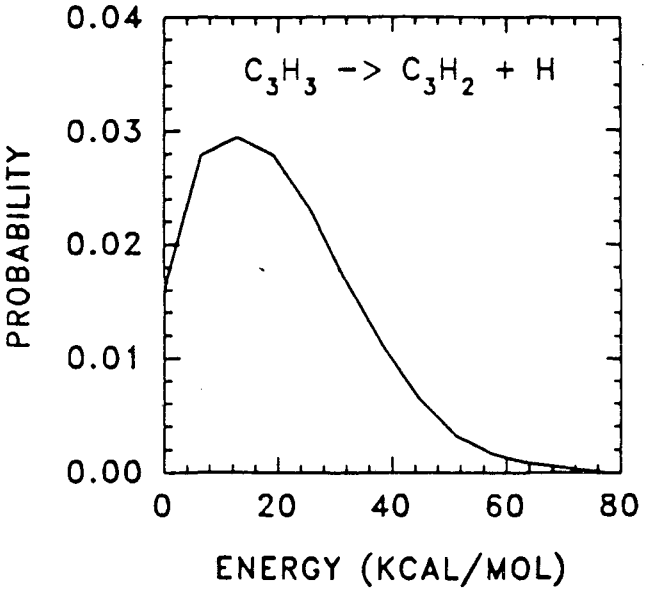
$C_3H_3 \rightarrow C_3H_2 + H$
PROBABILITY
0.04
0.03
0.02
0.01
0.00
0
20
40
60
80
ENERGY (KCAL/MOL)

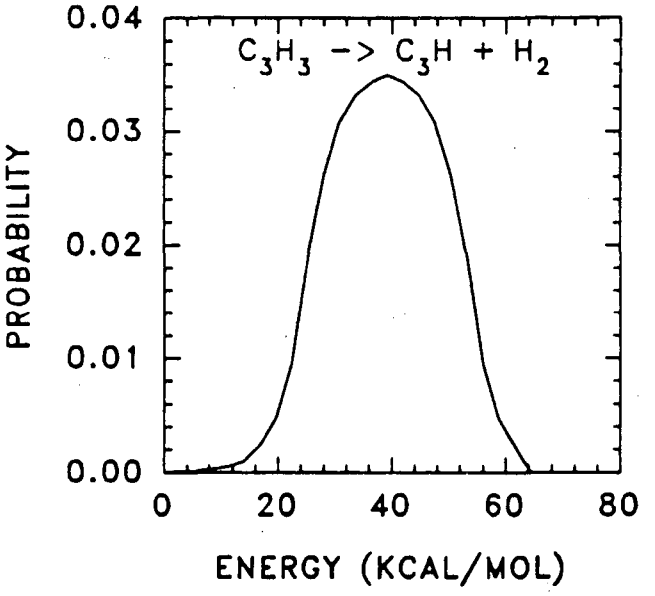
$C_3H_3 \rightarrow C_3H + H_2$
PROBABILITY
0.04
0.03
0.02
0.01
0.00
0
20
40
60
80
ENERGY (KCAL/MOL)

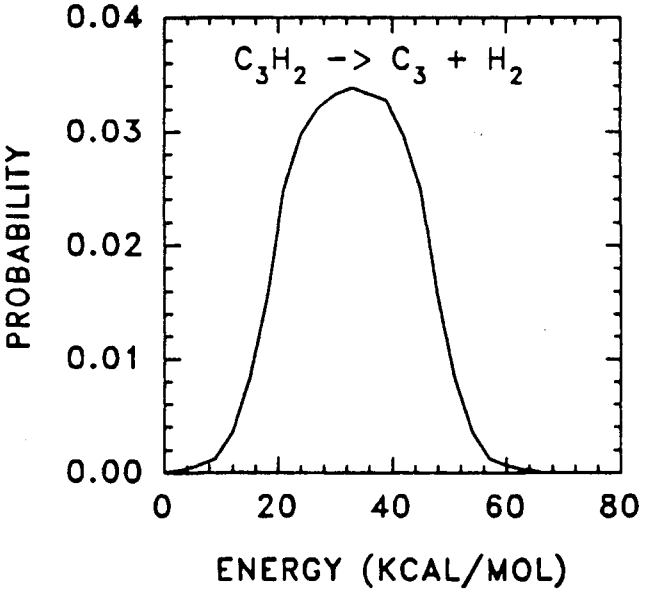
$C_3H_2 \rightarrow C_3 + H_2$
PROBABILITY
0.04
0.03
0.02
0.01
0.00
0
20
40
60
80
ENERGY (KCAL/MOL)

Fig. 6

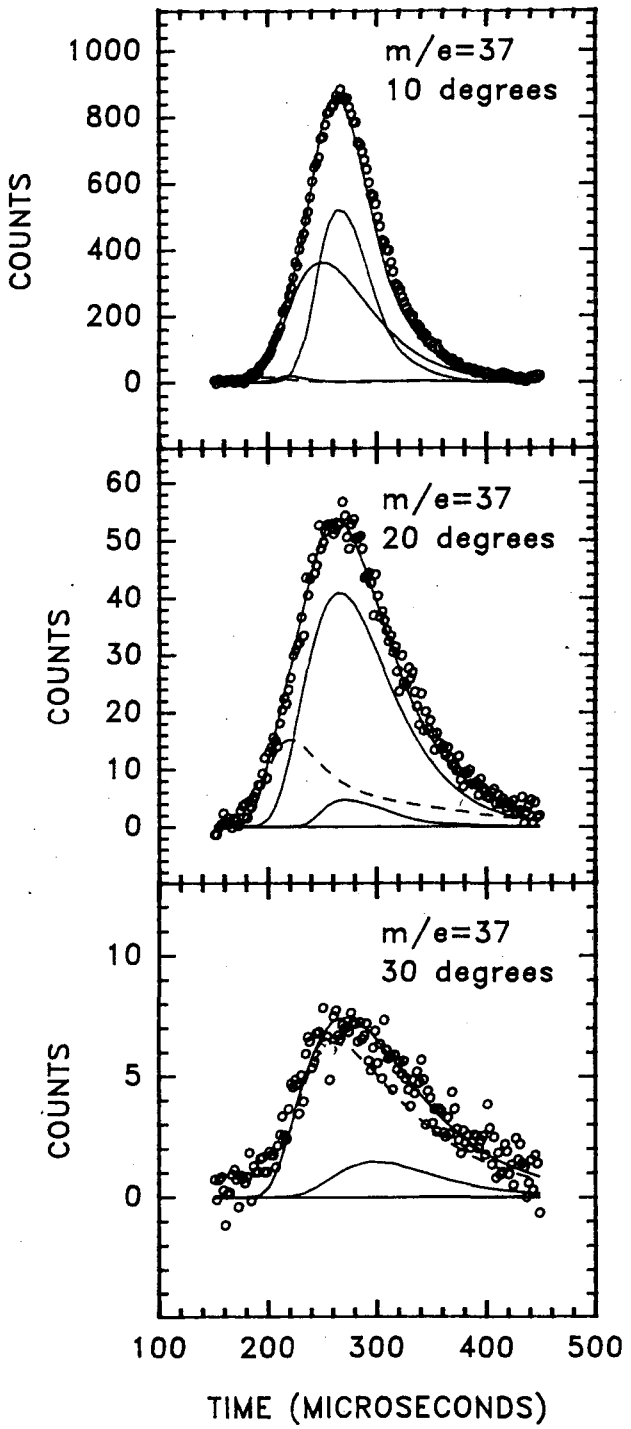
m/e=37
10 degrees
COUNTS
1000
800
600
400
200
0
m/e=37
20 degrees
COUNTS
60
50
40
30
20
10
0
m/e=37
30 degrees
COUNTS
10
5
0
100
200
300
400
500
TIME (MICROSECONDS)

Fig. 7

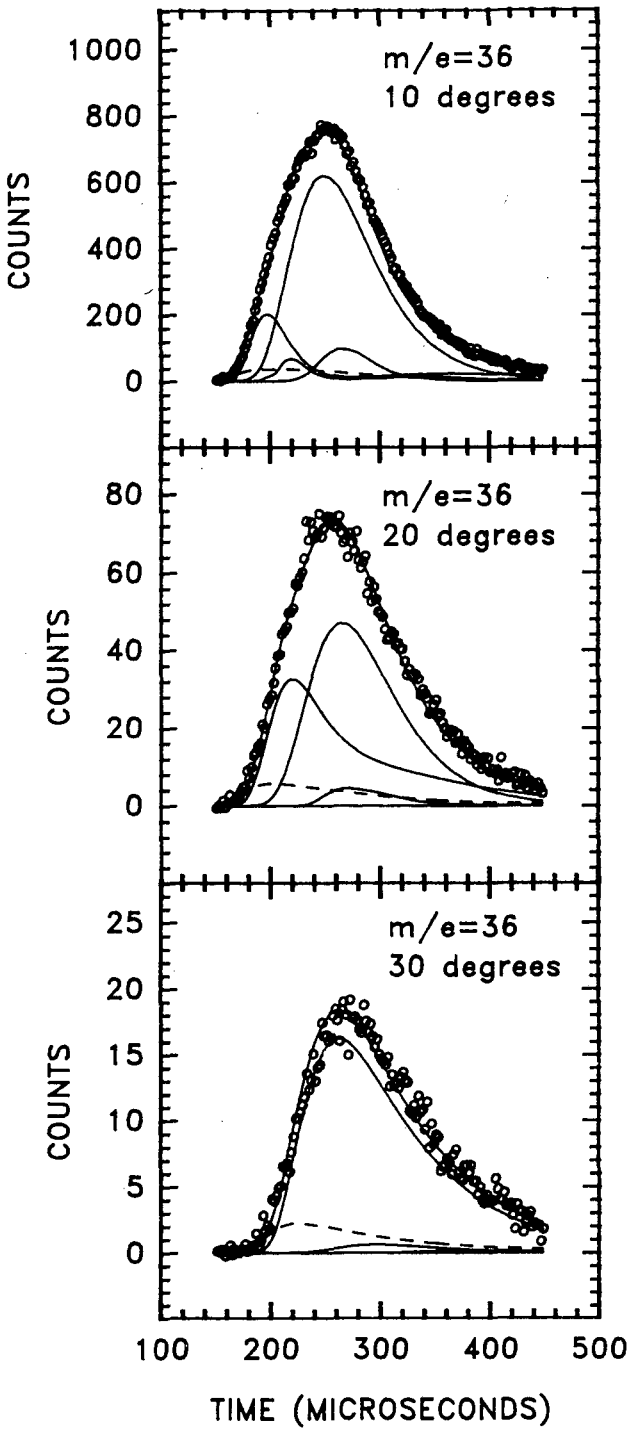
m/e=36
10 degrees
m/e=36
20 degrees
m/e=36
30 degrees
COUNTS
COUNTS
COUNTS
1000
800
600
400
200
0
80
60
40
20
0
25
20
15
10
5
0
100
200
300
400
500
TIME (MICROSECONDS)

Fig. 8

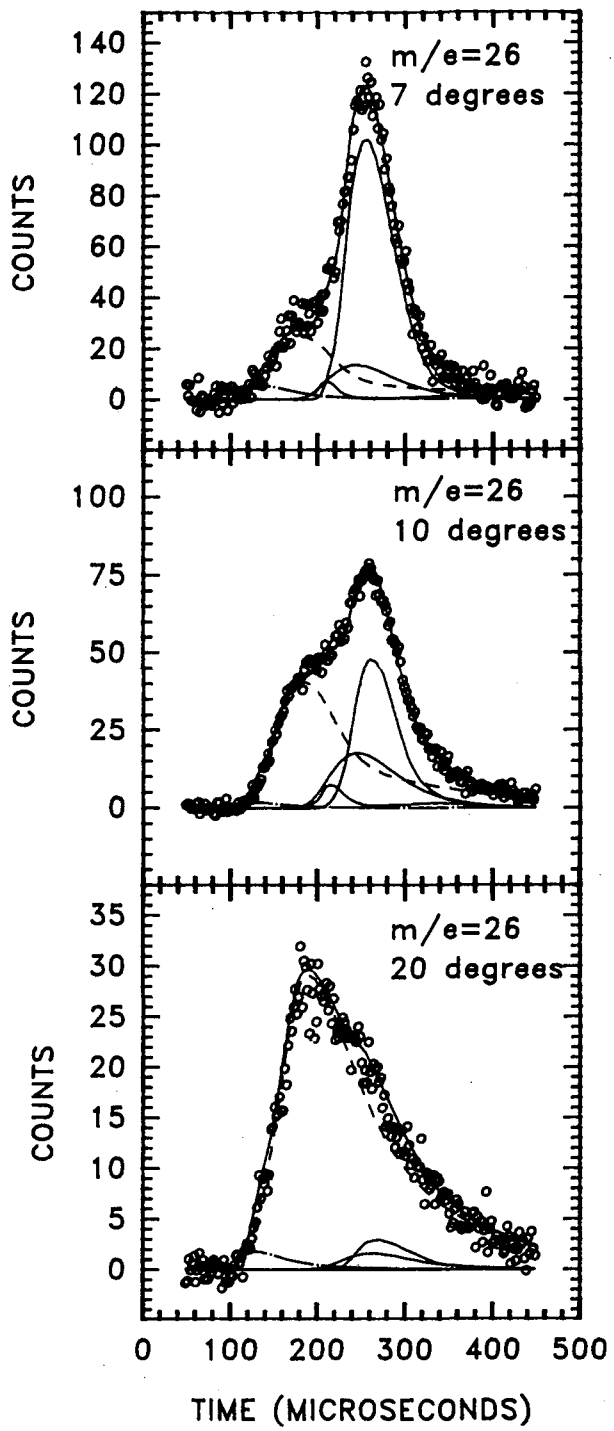
m/e=26
7 degrees
m/e=26
10 degrees
m/e=26
20 degrees
COUNTS
COUNTS
COUNTS
140
120
100
80
60
40
20
0
100
75
50
25
0
35
30
25
20
15
10
5
0
0
100
200
300
400
500
TIME (MICROSECONDS)

Fig. 9

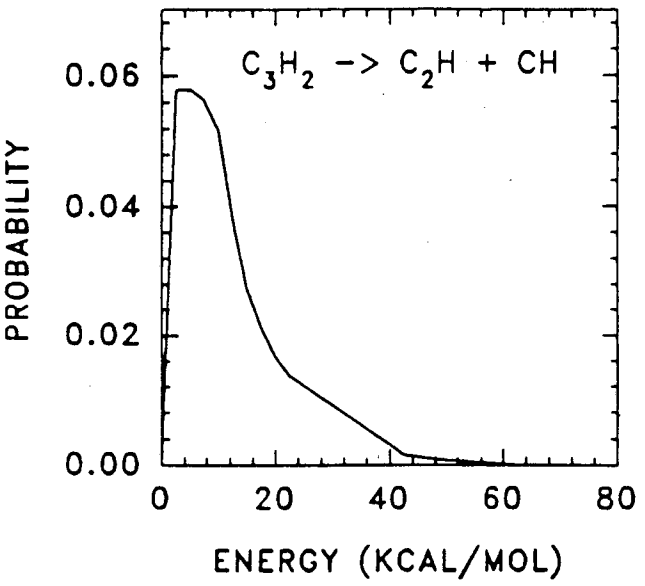
C_3H_2 -> C_2H + CH
PROBABILITY
0.06
0.04
0.02
0.00
0
20
40
60
80
ENERGY (KCAL/MOL)

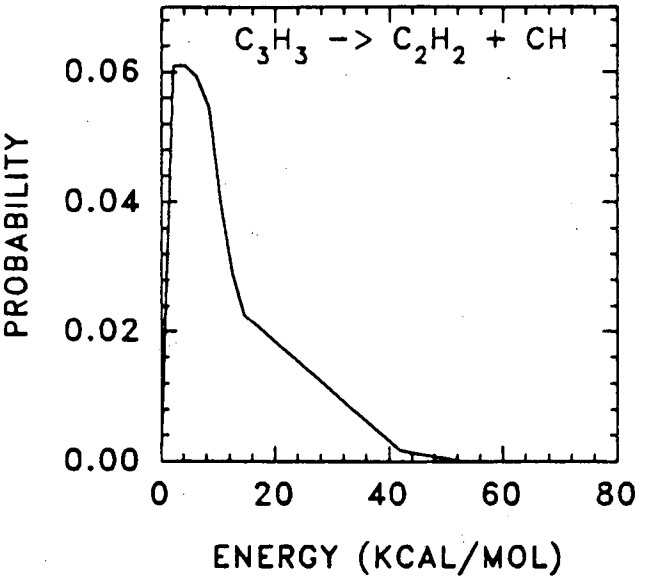
C_3H_3 -> C_2H_2 + CH
PROBABILITY
0.06
0.04
0.02
0.00
0
20
40
60
80
ENERGY (KCAL/MOL)

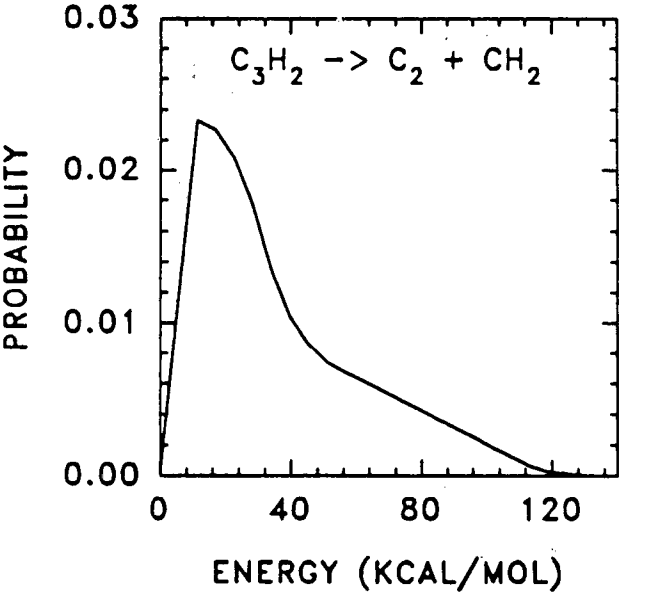
C_3H_2 -> C_2 + CH_2
PROBABILITY
0.03
0.02
0.01
0.00
0
40
80
120
ENERGY (KCAL/MOL)

Fig. 10

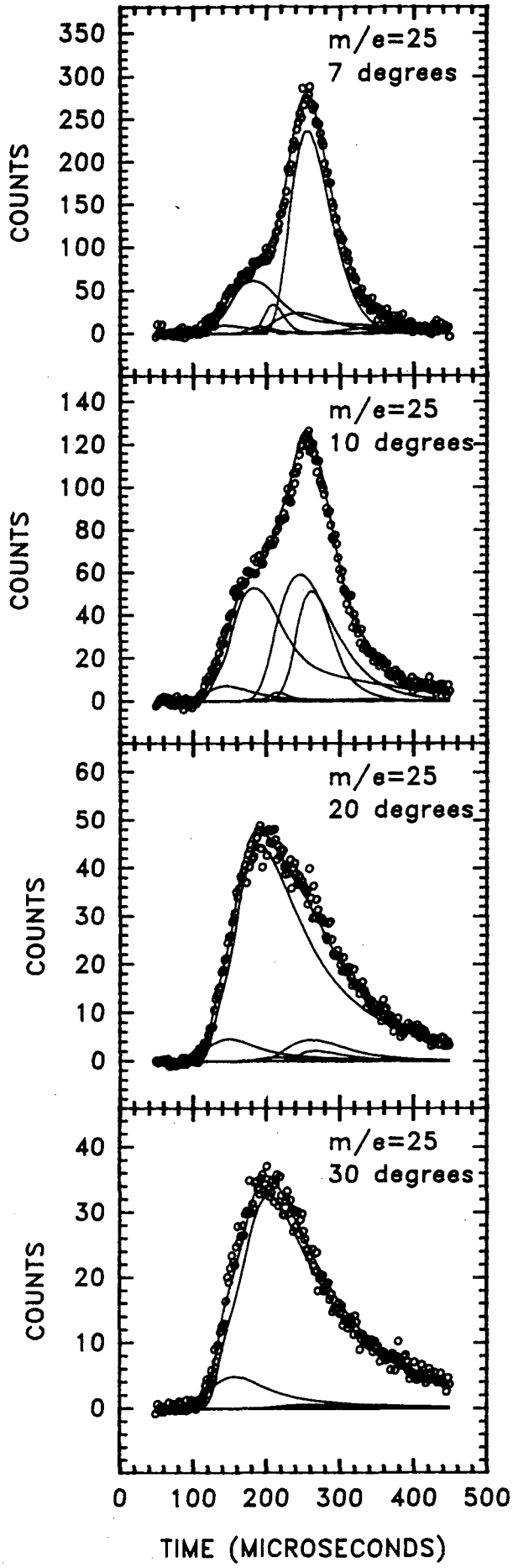
m/e=25
7 degrees
COUNTS
350
300
250
200
150
100
50
0
m/e=25
10 degrees
COUNTS
140
120
100
80
60
40
20
0
m/e=25
20 degrees
COUNTS
60
50
40
30
20
10
0
m/e=25
30 degrees
COUNTS
40
30
20
10
0
0
100
200
300
400
500
TIME (MICROSECONDS)

Fig. 11

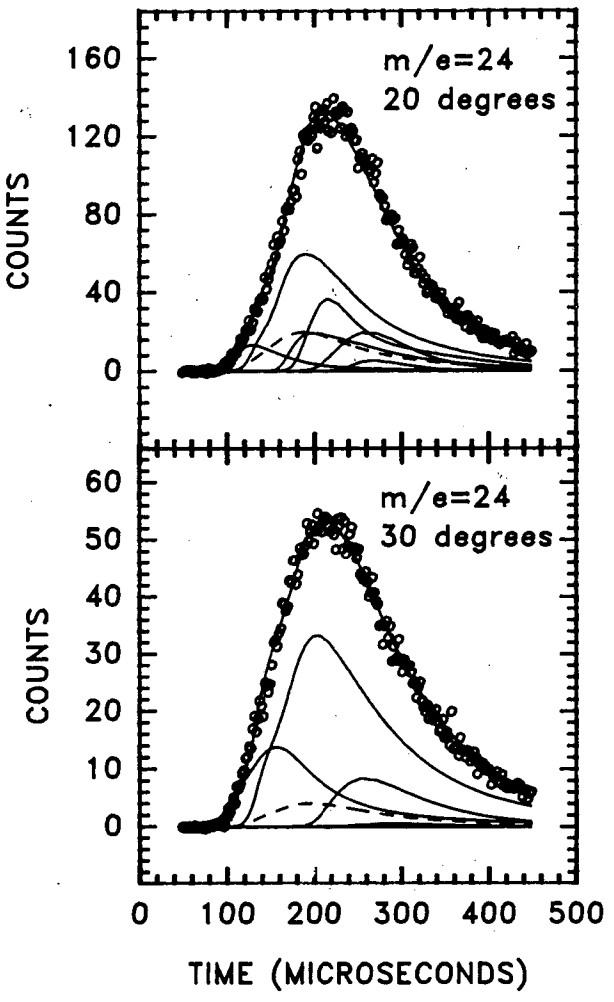
m/e=24
20 degrees
COUNTS
160
120
80
40
0
m/e=24
30 degrees
COUNTS
60
50
40
30
20
10
0
0
100
200
300
400
500
TIME (MICROSECONDS)

Fig. 12

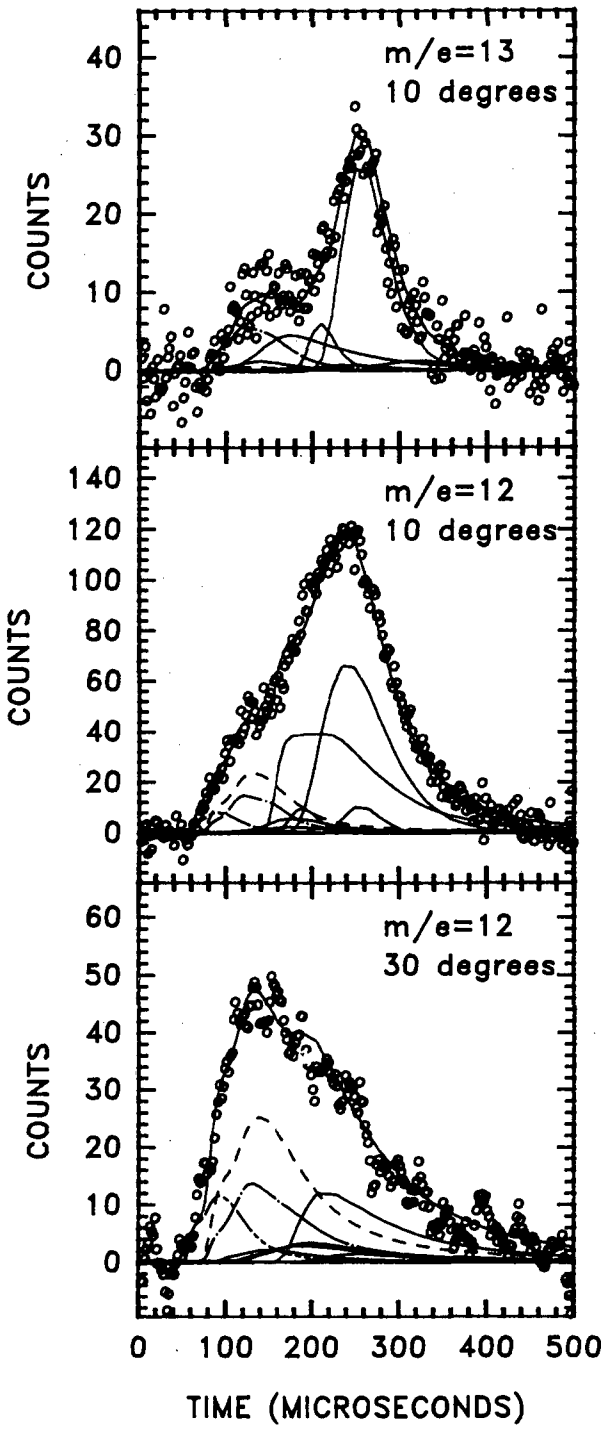
m/e=13
10 degrees
m/e=12
10 degrees
m/e=12
30 degrees
COUNTS
COUNTS
COUNTS
0
10
20
30
40
0
20
40
60
80
100
120
140
0
10
20
30
40
50
60
0
100
200
300
400
500
TIME (MICROSECONDS)

Fig. 13

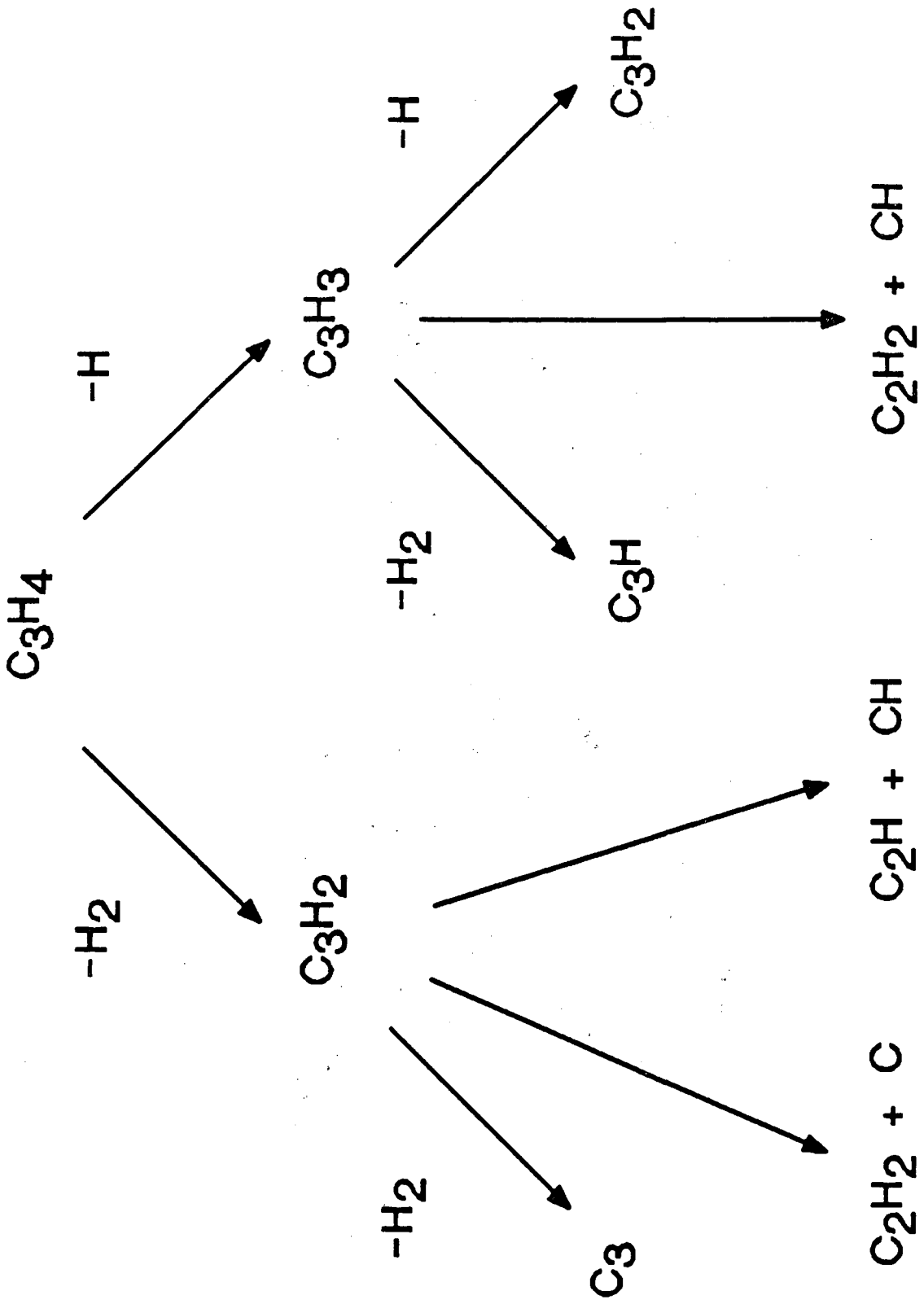

Fig. 14

LAWRENCE BERKELEY LABORATORY
UNIVERSITY OF CALIFORNIA
INFORMATION RESOURCES DEPARTMENT
BERKELEY, CALIFORNIA 94720